Simulating the 1998 spring bloom in Lake Michigan using a coupled physical-biological model

Lin Luo,[1,2] Jia Wang,[3] David J. Schwab,[3] Henry Vanderploeg,[3] George Leshkevich,[3] Xuezhi Bai,[2] Haoguo Hu,[2] and Dongxiao Wang[1]

Received 17 May 2012; revised 19 August 2012; accepted 4 September 2012; published 13 October 2012.

[1] A coupled physical-biological model is used to simulate the ecosystem characteristics in Lake Michigan. The physical model is the unstructured grid, Finite-Volume Coastal Ocean Model (FVCOM). The biological model is a NPZD model, including phosphorus as the nutrient, which is the limiting element in Lake Michigan, phytoplankton, zooplankton and detritus. The models are driven by observed hourly meteorological forcing in 1998 and the model results are calibrated by satellite and in situ data. The main physical and ecological phenomena in the spring of 1998 are captured. During March to May, a circle-like phytoplankton bloom appears in southern Lake Michigan, which looks like a 'doughnut'. The formation mechanisms of the prolonged spring bloom are investigated. It is confirmed that the phytoplankton bloom is forced by rapidly increasing temperature and light intensity in spring. The thermal front that develops in spring inhibits the transport of nutrients and phytoplankton from the nearshore to the deeper water. The wind-driven gyre circulation in southern Lake Michigan induces significant offshore transport, which contributes to the establishment of the circular bloom.

Citation: Luo, L., J. Wang, D. J. Schwab, H. Vanderploeg, G. Leshkevich, X. Bai, H. Hu, and D. Wang (2012), Simulating the 1998 spring bloom in Lake Michigan using a coupled physical-biological model, *J. Geophys. Res.*, *117*, C10011, doi:10.1029/2012JC008216.

1. Introduction

[2] Lake Michigan is the third-largest North American Great Lake with a surface area of 57,757 km^2 and a volume of 4,918 km^3. It is 491 km in length, 189 km in breadth, and 85 m in average depth (Figure 1). It is a typical phosphorus-limited lake system. Satellite imagery reveals that high chlorophyll concentrations appear in spring. This algal bloom in southern Lake Michigan (SLM) looks like a ring and thus is called a chlorophyll 'donut' ring [*Budd et al.*, 2002; *Kerfoot et al.*, 2008]. This phenomenon is regarded as the result of coupled physical and biological processes: Lake Michigan is a nearly enclosed basin with a sloping bottom in the north and south parts of the lake (Figure 1). As a result, the shallow coastal waters warm up first and are separated from the cool water in central areas by a sharp thermal front during the spring. The front inhibits the offshore transport of material [*Beletsky and Schwab*, 2001; *Ullman et al.*, 1998; *Bolgrien and Brooks*, 1992]. The wind-driven circulation is dominant in Lake Michigan, which causes the cross-frontal transport of material under favorable meteorological forcing [*Tarapchak and Rubitschun*, 1981; *Beletsky et al.*, 1999, 2003]. The two physical mechanisms have reverse, competitive effects on the offshore transport from the coastal water to the mid-lake area. *Vanderploeg et al.* [2007] and *Kerfoot et al.* [2008] uncovered the columnar patterns for the complex chlorophyll bloom and other variables by cross-lake surveys. They investigated the relationship between the meteorological forcing and biological fields and emphasized that winter storms had a remarkable effect on the planktonic food web during the late winter and spring.

[3] *Ji et al.* [2002] and *Chen et al.* [2004] conducted modeling studies of the interactions between the resuspension event and phytoplankton in SLM. Their simulation studies focused only on blooms in March, and the time scale was restricted to 5–7 days. Specifically, they simulated and examined the influence of episodic resuspension plume events on the spring bloom in March using a 7-component coupled biological and physical model. The stormy weather driving the suspended sediment plumes was emphasized. However, from the satellite images, the bloom ring was observed to last for two whole months, eventually disappearing in May 1998. Based on the empirical observations, it is natural to ask whether the sediments suspended by a storm on the time scale of several days are the only source of nutrients to the spring bloom? What is the mechanism that sustains the spring bloom for as long as two months? Will the chlorophyll 'donut' still occur without the supply of nutrients from riverine loading and sediment release due to the storm?

[1]State Key Laboratory of Tropical Oceanography, South China Sea Institute of Oceanology, Chinese Academy of Sciences, Guangzhou, China.
[2]Cooperative Institute for Limnology and Ecosystems Research, University of Michigan, Ann Arbor, Michigan, USA.
[3]NOAA Great Lakes Environmental Research Laboratory, Ann Arbor, Michigan, USA.

Corresponding author: L. Luo, State Key Laboratory of Tropical Oceanography, South China Sea Institute of Oceanology, Chinese Academy of Science, 510301 Guangzhou, China. (luolin@scsio.ac.cn)

0148-0227/12/2012JC008216

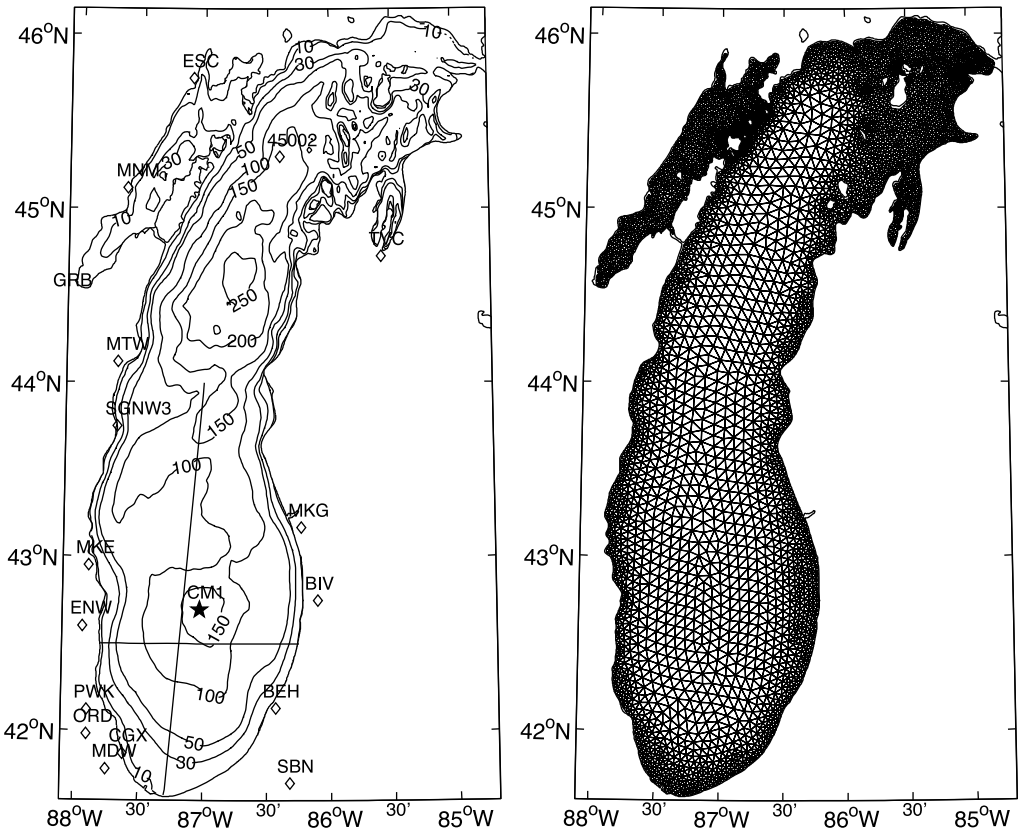

Figure 1. (left) The topography of Lake Michigan and the observation station locations: solid pentagram, thermistor mooring; open diamond, meteorological stations. Transects N-S and W-E are indicated. (right) Model grid.

[4] In this paper, we examine the processes of the spring bloom formation and decay from March to May 1998. Using a state-of-the-art 3-D coupled physical-biological model, FVCOM, we simulate the development of the 1998 spring bloom to investigate the relationship between the structure of the spring bloom and physical and biological forcing, and to search for the mechanisms of this phenomenon over a long time scale during March to May, differing from the previous studies of the short-term (5–7 days in March) bloom processes [*Ji et al.*, 2002; *Chen et al.*, 2004]. To test the importance of general circulation and interior source of ecological factors in the lake for sustaining the donut-like spring bloom, the phosphorus released from suspended sediments and rivers are excluded from this study.

[5] The remaining sections are organized as follows. The coupled physical-biological model, forcing, and data used to validate the model are described in Section 2. The primary results of the model along with measurements are presented in Section 3. The impacts of physical and biological processes on the spring bloom are discussed in Section 4. Last, the conclusions are summarized in Section 5.

2. Methods and Data

2.1. Physical Model

[6] A three-dimensional coupled physical-biological model of Lake Michigan is used to simulate the ecosystem processes in Lake Michigan. The model is based on an unstructured grid, Finite-Volume Coastal Ocean Model (FVCOM) developed by *Chen et al.* [2006]. FVCOM has the following features: 1) unstructured triangular mesh in the horizontal to represent the complex geometry; 2) σ-coordinate in the vertical to represent the irregular bottom topography; 3) free surface; 4) energy conserving using the finite volume method; 5) *Mellor and Yamada* [1982] level 2.5 turbulent closure scheme for vertical mixing; and 6) Smagorinsky turbulent closure scheme for horizontal mixing. The model has been successfully applied to study several estuaries and shelf regions [*Weisberg and Zheng*, 2006; *Yang and Khangaonkar*, 2008; *Ji et al.*, 2008].

[7] In the physical model, we implement the wind-wave mixing parameterization newly developed by *Hu and Wang* [2010] to accurately simulate the mixed layer depth

$$K_{mw} = \frac{2\upsilon^2}{g}\delta\beta^3 W^3 e^{\frac{gz}{\beta^2 W^2}} \quad (1)$$

where K_{mw} is the wave-induced mixing coefficient; β is the wave age ($0 < \beta < 1$ for growing wave, and $\beta = 1$ for mature wave), δ is the wave steepness ($\delta = 2\alpha/\lambda$, α is the amplitude and λ is the wavelength), W is the wind speed, $z < 0$ is the depth, $\upsilon = 0.4$ is the von Kármán constant, and g is acceleration of gravity. In this study, a mature but not breaking

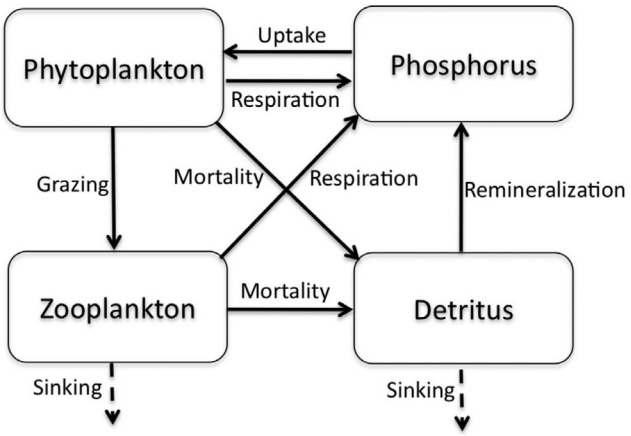

Figure 2. Schematic of the NPZD model in Lake Michigan.

wave is assumed as $\beta = 0.4$, $\delta = 0.16$. The heat diffusion coefficient K_{hw} is assumed here to be equal to K_{mw}.

[8] Then, the total vertical mixing coefficients are

$$K'_m = K_m + K_{mw}; K'_h = K_h + K_{hw} \tag{2}$$

where K_m and K_h are calculated by the level 2.5 closure turbulence model.

2.2. Biological Model

[9] The biological model implemented in FVCOM is a Flexible Biological Module. To simplify the biological processes we choose four compartments, including phosphorus as the nutrient (N), which is the limiting element in Lake Michigan, phytoplankton (P), zooplankton (Z), and detritus (D), to establish a NPZD model in Lake Michigan (Figure 2). The governing equations for the biological variables are given as

$$\frac{\partial N}{\partial t} + u\frac{\partial N}{\partial x} + v\frac{\partial N}{\partial y} + w\frac{\partial N}{\partial z} - \frac{\partial}{\partial z}\left(A_h\frac{\partial N}{\partial z}\right) = -P(uptake) + Z(respiration) + P(respiration) + D(remineralization) \tag{3}$$

$$\frac{\partial P}{\partial t} + u\frac{\partial P}{\partial x} + v\frac{\partial P}{\partial y} + w\frac{\partial P}{\partial z} - \frac{\partial}{\partial z}\left(A_h\frac{\partial P}{\partial z}\right) = P(uptake) - P(respiration) - P(mortality) - ZP(grazing) - P(sinking) \tag{4}$$

$$\frac{\partial Z}{\partial t} + u\frac{\partial Z}{\partial x} + v\frac{\partial Z}{\partial y} + w\frac{\partial Z}{\partial z} - \frac{\partial}{\partial z}\left(A_h\frac{\partial Z}{\partial z}\right) = ZP(grazing) + ZD(grazing) - Z(respiration) - Z(mortality) \tag{5}$$

$$\frac{\partial D}{\partial t} + u\frac{\partial D}{\partial x} + v\frac{\partial D}{\partial y} + w\frac{\partial D}{\partial z} - \frac{\partial}{\partial z}\left(A_h\frac{\partial D}{\partial z}\right) = P(mortality) + Z(mortality) + D(grasing\ \ loss) - ZD(grazing) - D(remineralization) - D(sinking) \tag{6}$$

In the derivative operator, x, y, and z are the eastward, northward, and vertical axes of the Cartesian coordinate, and u, v, and w are the x, y, and z components of the velocity. A_h is the thermal diffusion coefficient. The biological parameters and initial conditions of the biological variables are set according to previous literature values [*Chen et al.*, 2002, 2004]. The initial conditions of N, P Z, and D were given as 0.1 mmol P/m^3, 0.5 mmol C/m^3, 0.7 mmol C/m^3, and 6.5 mmol C/m^3. Details of the biological models are given in Appendix A, and the parameters used are listed in Table 1. The concentration of chlorophyll is derived from the phytoplankton as a ratio of chlorophyll to carbon in phytoplankton, which is also listed in Table 1.

2.3. Model Setting

[10] The bathymetry of Lake Michigan is interpolated from the NOAA National Geophysical Data Center (http://www.ngdc.noaa.gov/mgg/greatlakes/greatlakes.html). There are a total of 9054 elements and 4981 nodes in the horizontal (Figure 1), and 21 sigma levels in the vertical. The resolution is higher near the surface and the bottom boundary layer. Based on the global linear stability criteria proposed by *Wang* [1996], the minimum depth was set to 5 m according to the stability condition, $h_{\min} + \zeta_{\max} > 0$ where $h_{\min}$ is the minimum water depth, and $\zeta_{\max}$ is the maximum water elevation possibly caused by strong (gust) winds and storm surges along the coast. Based on the CFL criterion, one of the global stability conditions, the internal mode time step of the numerical integration is 180 s, while the external mode time step is 18 s.

[11] The biological model is run simultaneously with the physical model. The model was spun up over 2 months, starting on January 1, 1998. The year 1998 was chosen because it is a typical year with a vivid donut-like spring bloom. Also we have systematic measurements in 1998 including satellite and in situ measurements from the Episodic Event-Great Lakes Experiments (EEGLE) project (http://www.glerl.noaa.gov/eegle/data/data.html) that measured both physical and biological variables. The model is driven by observed hourly winds and heat flux taken from the meteorological stations around Lake Michigan (Figure 1). The heat flux includes two parts: the surface net heat flux and the penetrated short-wave irradiance. The initial conditions of biological variables are uniform since the water column is vertically well mixed in winter. The phosphorus released from the suspended sediments is not taken into account. To test the hypothesis that the donut-

Table 1. Biological Model Parameters

Parameter	Definition	Value Used
$\mu^P_{\max}$	Maximum growth rate for P	2.8 d^{-1}
K_s	Half-saturation constant for the N uptake by P	0.6 mmol P m^{-1}
γ_Z	Zoo respiration coeffcient	0.015d^{-1}
γ_P	Phyto respiration coeffcient	0.01d^{-1}
γ^T	Exponential for Temperature forcing	0.07
d^R	Remineralization rate of detritus	0.015 d^{-1}
$G_{\max}$	Maximum P grazing rate by Z	0.4 d^{-1}
σ_P	Preference coefficient of Z on P	0.5 (mmol C m^{-3}) $^{-1}$
σ_D	Preference coefficient of Z on D	0.1 (mmol C m^{-3}) $^{-1}$
ε^Z	Assimilation efficiency of Z	0.35
ε_P	Mortality rate of P	0.01 d^{-1}
ε_Z	Mortality rate of Z	0.02 d^{-1}
$\lambda_{\text{Chl:C}}$	Ratio of chlorophyll to carbon (C)	0.34 mg Chl/mmol C
w_P	Sinking velocity of P	0.6 m d^{-1}
w_D	Sinking velocity of D	0.6 m d^{-1}

like spring bloom is sustained by physical-biological processes in addition to riverine nutrients, we exclude the river input in this model.

2.4. Calibration Data

[12] Satellite-measured water surface temperature is derived from GLSEA (Great Lakes Surface Environmental Analysis, http://coastwatch.glerl.noaa.gov/glsea/glsea.html) and satellite-retrieved chlorophyll concentration is derived from SeaWifs (Sea-viewing Wide field-of-view sensor, http://oceandata.sci.gsfc.nasa.gov/SeaWiFS). The satellite measurements are used to validate the seasonal variations and spatial patterns of the simulated water surface temperature and chlorophyll concentration. In situ temperature measurements deployed by a mid-lake thermistor mooring are used to validate the vertical distribution of water temperature.

[13] To measure the model's skill for reproducing the measurements, two statistical measures are introduced to conduct the model-data comparison. Mean bias deviation (MBD) is defined as

$$MBD = 100\frac{\frac{1}{n}\sum_{i=1}^{n}(x_i - y_i)}{\frac{1}{n}\sum_{i=1}^{n} y_i} = 100\frac{\bar{X} - \bar{Y}}{\bar{Y}} \quad (7)$$

and root mean square deviation (RMSD) is defined as

$$RMSD = \left[\frac{\sum_{i=1}^{n}(x_i - y_i)^2}{n}\right]^{1/2} \quad (8)$$

where x_i and y_i (i = 1, 2, 3, … n) are the modeled and observed time series of any variables such as T, Chl, etc., n is the total sampling number, and the overbars denote the average of the time series. MBD directly measures the relative bias or error of the modeled time series from the observed in percentage. RMSD measures the absolute error of the modeled time series against observation.

3. Results

3.1. Lake Circulation and Temperature

3.1.1. General Circulation

[14] The model reproduces a counterclockwise-rotating (cyclonic) gyre, which persists from March to May in the southern lake (Figure 3). The maximum speed of the strong coastal currents is 9 cm s-1 in March. The mean depth-averaged speed is 2 cm s^{-1}. Then it weakens in April and is weakest in May with a mean depth-averaged speed of less than 1 cm s^{-1} and a maximum speed of 4.8 cm s^{-1}. The simulated circulation pattern agrees with results of long-term current observations (Figure 3) and previous simulations in that the circulation pattern tends to be cyclonic in Lake Michigan, and the currents of March and April are stronger than May [*Beletsky et al.*, 1999; *Beletsky and Schwab*, 2001]. This cyclonic structure of circulation exists during the entire spring period, which provides a pathway for the westward transport of material from the east coast to the mid-lake area.

[15] The circle-like current is clear in the west-east and north-south transect of velocity: The meridional velocity is southward in the west and reversed in the east (Figure 9b). The zonal velocity is eastward in the south and westward in the mid-lake area (Figure 10b). The velocity is vertically uniform in the deep basin and slightly increases from surface to the bottom in shallow waters due to interactions with bottom topography.

3.1.2. Temperature

[16] The simulated temperature is in good agreement with the observations (Figure 4). During March to May, the temperature increases. In March, the central lake is warmer than the coastal water, and the highest temperature appears in the central part of the southern basin, which is due to the shallow coastal waters cools down faster during the winter, whereas in March, the air temperature is still cold with a monthly mean surface temperature lower than 2°C [*Wang et al.*, 2010]. In April, the lake surface temperature becomes warmer, and the highest temperature reaches 10°C, particularly along the southern coast. The temperature difference between the southern and northern lake is great (5°C). In May, the highest temperature shifts to eastern SLM; all the coastal water around the lake including Green Bay becomes warmer due to constant surface solar heating. The model captures the spatial temperature pattern. However, the simulated low surface temperature area in the northern Lake Michigan basin is smaller than the observed, implying that a missing ice component in the model leads to faster warming in the lake [*Wang et al.*, 2010].

[17] Figure 5 shows the lakewide average surface temperature calculated by the model with and without the wind-wave mixing scheme and observed by satellite. The seasonal cycle of lake surface temperature is well reproduced by the model embedded with the wind-wave mixing parameterization, with MBD being 1.2% and RMSD being 1.4°C, since discrepancies exist in summer and fall. Without the wind-wave mixing parameterization, the simulated temperature is underestimated, with MBD being −5.75% and RMSD being 1.85°C.

[18] The model reproduces the basic features of thermal structure evolution in Lake Michigan (Figure 6). The water is well mixed from the surface to the bottom in late winter and spring at near 4°C. Stratification develops in summer, and the thermocline deepens in fall. The water column is well mixed again in winter due to atmospheric cooling. Comparing observations to the modeled results, it is found that without the wind-wave mixing, the upper mixed layer is shallow, and the thermocline is weak, while the model with the wind-wave mixing scheme produces a more accurate representation of the mixed layer depth of 15 m in summer. With a strong gradient, the seasonal thermocline appears at the depths of 15–25 m. This indicates that the wind plays an important role in the thermocline formation and maintenance, and the wind wave mixing parameterization works well in Lake Michigan.

3.2. Spring Bloom and Other Biological Variables

[19] The observed and simulated phytoplankton patterns are shown in Figure 7. During March to May, phytoplankton grows with the increasing temperature. In March, the chlorophyll concentration is high, and satellite images show the 'donut' formation in SLM; however in our simulation, the March bloom is just along the coast, but not obvious in northern SLM. The model cannot reproduce the closed 'donut' ring in March, and the high chlorophyll concentration only appears in coastal waters, which will be explained in

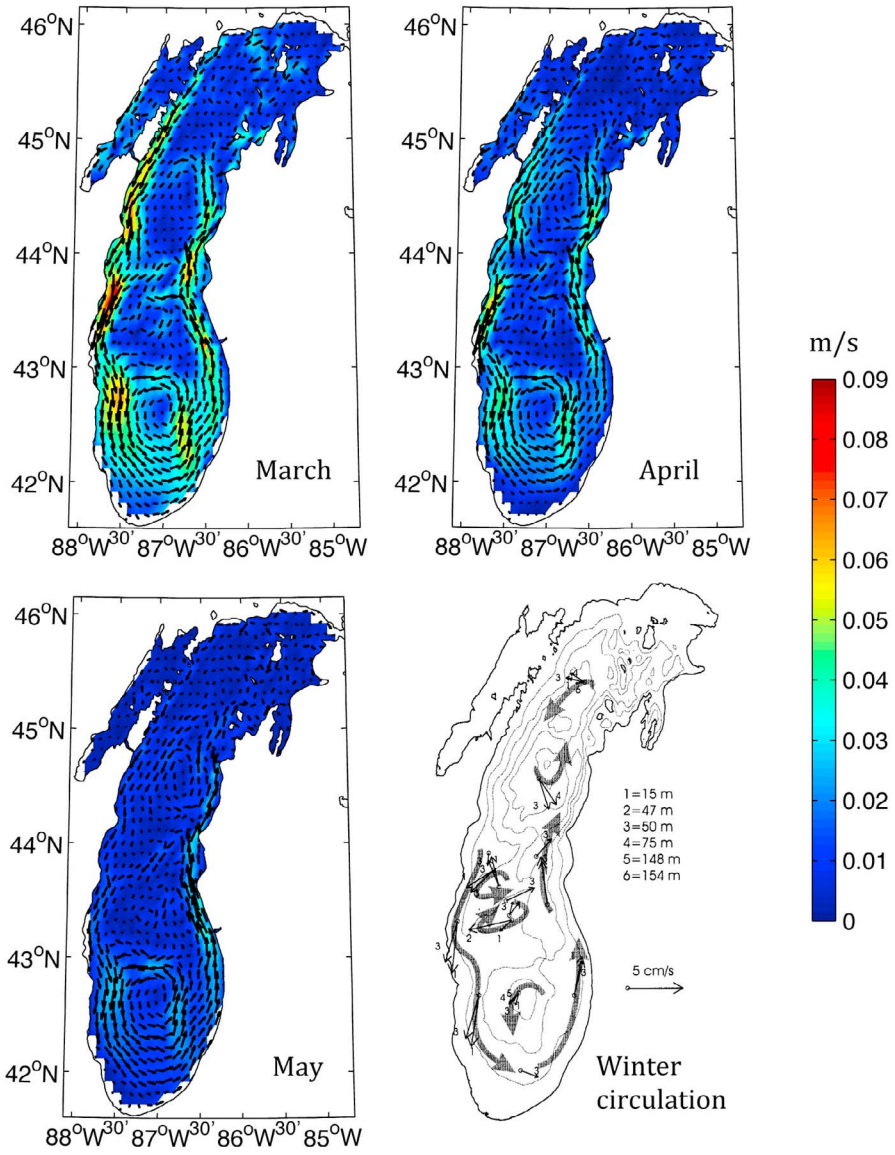

Figure 3. The monthly mean depth-averaged current (m/s) of Lake Michigan in March, April, and May and winter circulation derived from observation [*Beletsky et al.*, 1999].

the next section. The donut exists in SLM in the satellite image in April, and our simulation reproduces it well. The 'donut' spring bloom in both satellite and simulated images decays in May, though the concentration of chlorophyll is still high in this month (Figures 7 and 8). The simulated chlorophyll concentration shows 20% higher in the central basin than the observed in May, which may be the growth rate of phytoplankton keeps high in this month and the phytoplankton in the south and north basin increases lagging behind that in the coastal shallow waters. And for lack of additional supply of nutrient, the phytoplankton in coast area decreased. This phenomenon also can be seen in June.

[20] Figure 8 shows the seasonal cycle of chlorophyll concentration in the surface layer. The model captures two phytoplankton peaks, which appear in spring and autumn. The discrepancy between the simulation and satellite data is large with MBD being −19.55%, and RMSD being 0.37 mg/m^3. It may be that we take no account of the external nutrient input from river and sediments. However, the simulated results indicate that the simulation matches with the seasonal variability of phytoplankton.

[21] The typical formation of the 'donut' structure can be seen clearly from two transects from west-east and north-south directions. Along the west-east section (Figure 9), the high chlorophyll concentration appears in the shallow water in both the west and the east sides of SLM corresponding to the warmer water and stratification appearing in these areas. Accordingly, nutrient is consumed and dramatically decreases due to the rapid growth of phytoplankton along the coast. In the deep central basin, the nutrient concentration is high

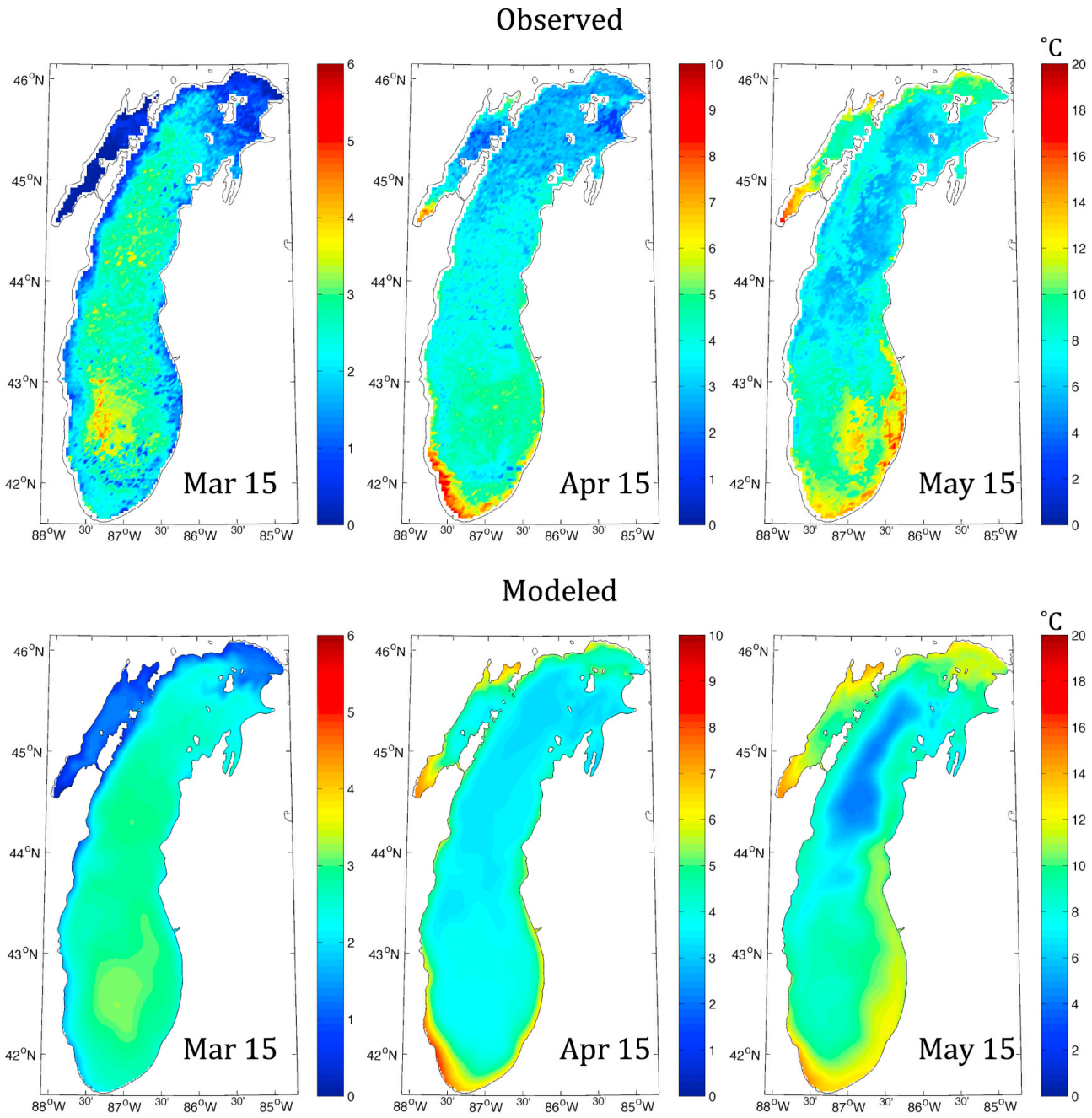

Figure 4. GLSEA satellite image and simulated daily averaged water surface temperature (°C) on March 15, April 15, and May 15, 1998 in Lake Michigan.

because less phytoplankton grows due to lower temperature and lack of solar radiation. Zooplankton has a similar and laggard growth pattern as phytoplankton, depending on phytoplankton grazing. Detritus is high in the bottom of coastal waters, since it results from the mortality of zooplankton and phytoplankton.

[22] Along the north-south section (Figure 10), south coastal water is warm with stratification, which leads to a phytoplankton bloom and nutrient consumption. High chlorophyll concentration also occurs on the mid-ridge of SLM. However, the pattern of low-nutrient, high-zooplankton in the surface layer and high-detritus in the bottom layer in this area is not as obvious as in the coastal water, implying that the mechanism and source of the phytoplankton bloom is not the same as along the coast.

[23] The seasonal cycle of the four biological elements is show in Figure 11. There is a negative relation between the concentration of chlorophyll and phosphorus, since the growth of phytoplankton consumes the nutrient. The increase of zooplankton and detritus lag behind the phytoplankton bloom, since the zooplankton grows by grazing the phytoplankton, and detritus comes from the mortality of phytoplankton and

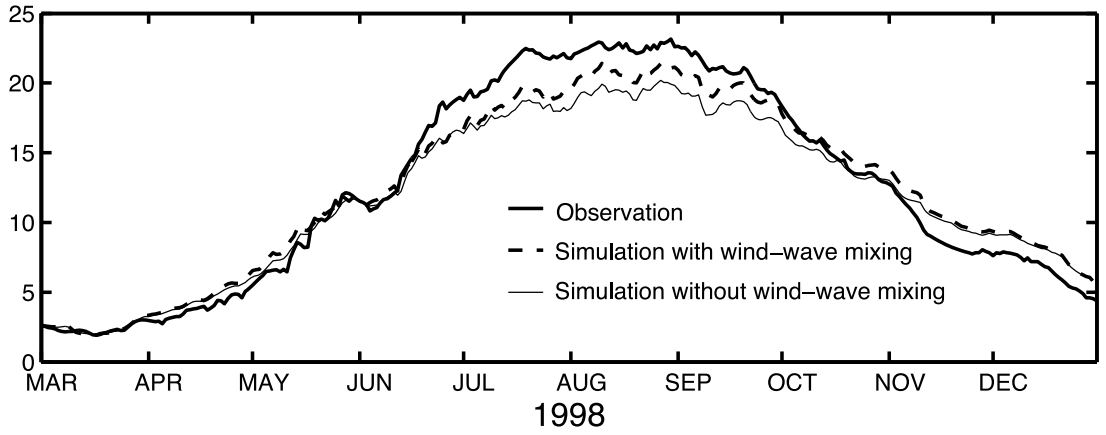

Figure 5. Temporal (daily) comparison of the domain-averaged surface temperature (°C) between the GLSEA2 measurement (thick solid) and simulated by FVCOM with (dashed) and without wind-wave mixing scheme (thin solid) during March to December 1998.

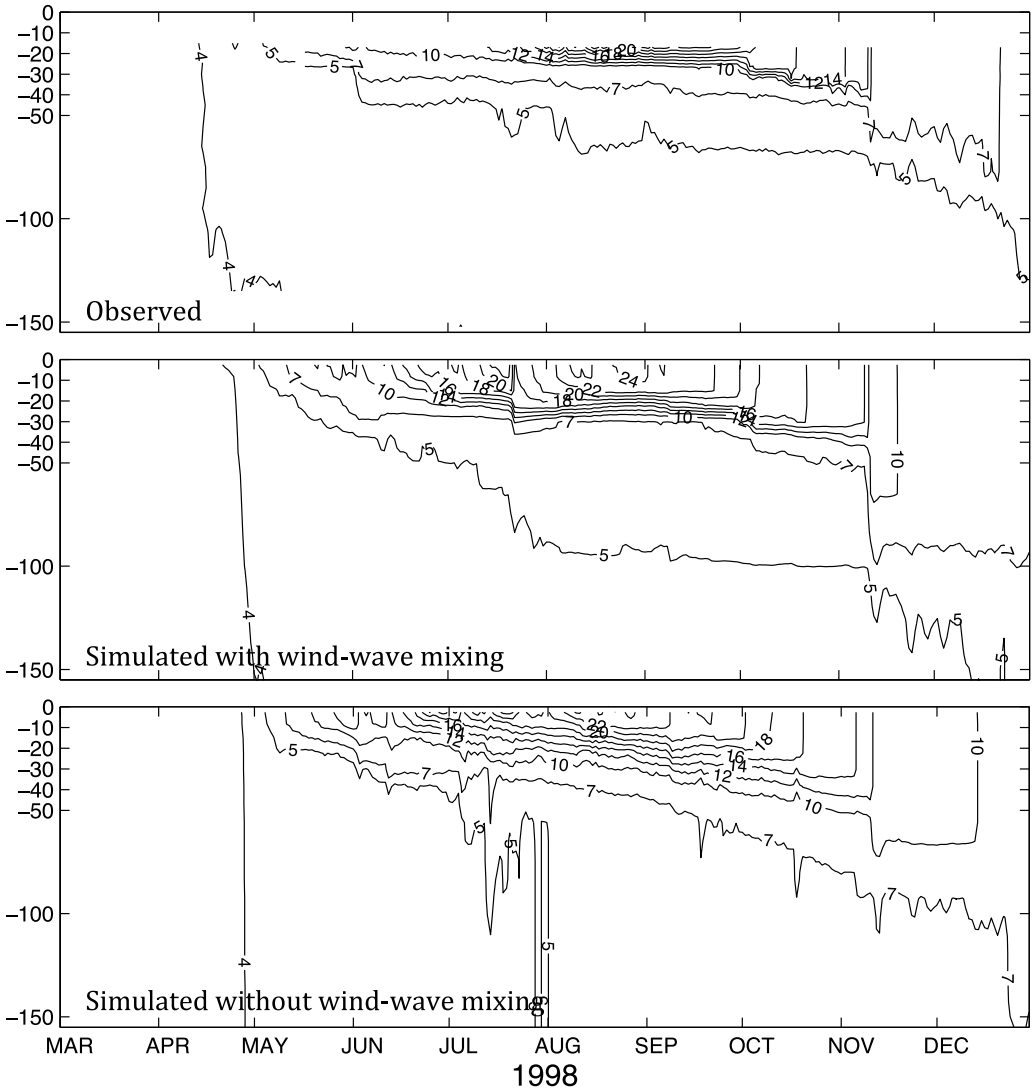

Figure 6. Observed and simulated (with and without wind-wave mixing scheme) water temperature profile (°C) in CM1 from March to December 1998.

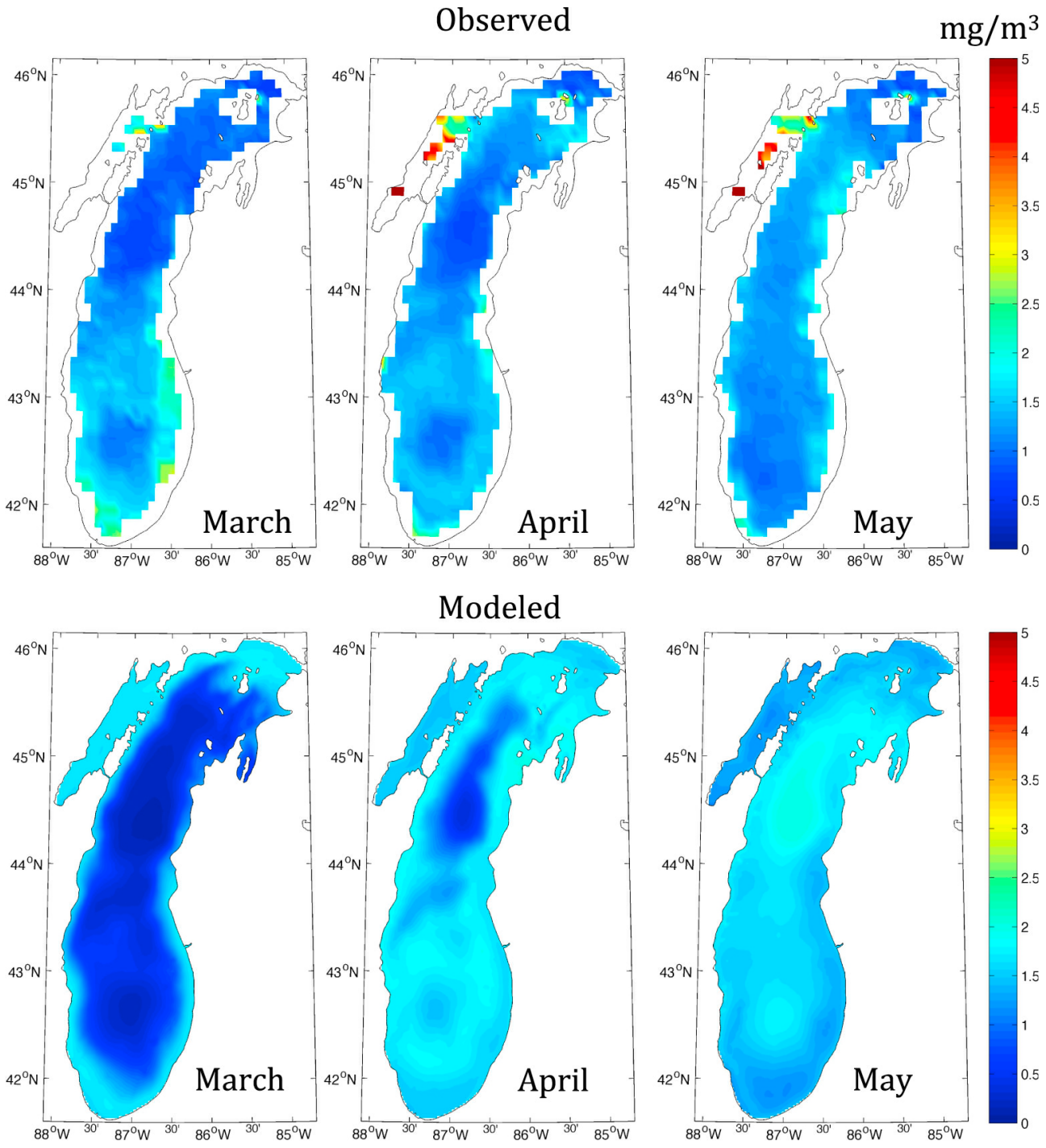

Figure 7. Monthly averaged SeaWiFS image and simulated surface chlorophyll concentration (mg/m3) in March, April, and May 1998.

zooplankton. The model results match observations by *Vanderploeg et al.* [2012].

4. Mechanisms Responsible for the 'Donut-Like' Spring Bloom

[24] The biological model is based on the fact that the gross growth rate of phytoplankton depends on several key factors. In this model, three factors are considered: light intensity, water temperature, and nutrient limitation. The empirical formula is given as

$$\mu = \mu(T) \bullet \mu(I) \bullet \mu(N) \tag{9}$$

where

$$\mu(T) = \exp\left(-\alpha_T \left| T - T_{opt} \right|\right) \tag{10}$$

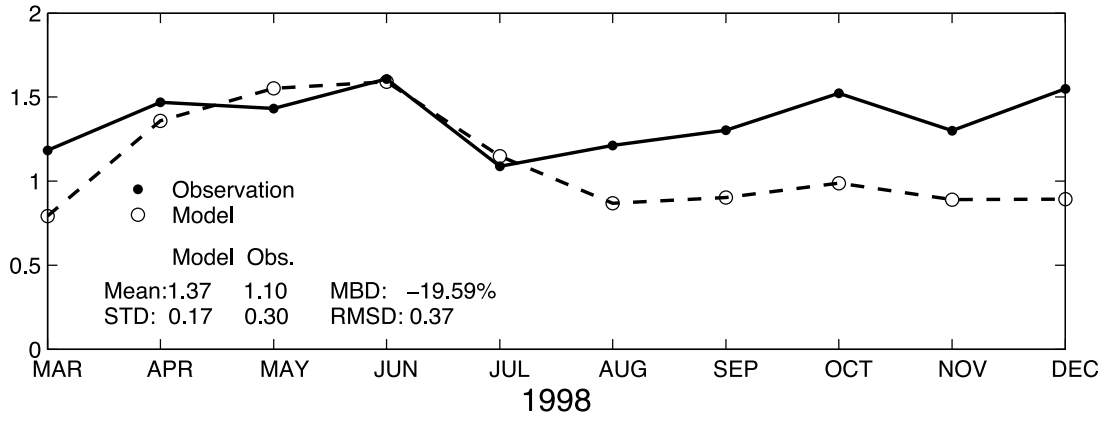

Figure 8. Temporal (monthly) comparison of the domain-averaged surface chlorophyll concentration (mg/m^3) between the FVCOM simulated (circle) and SeaWiFS measurement (dot) during March to December 1998. The simulated and observed mean and standard deviation, and MBD and RMSD are provided.

$$\mu(I) = \left(1 - e^{-\frac{\alpha_I I}{\mu_{\max}}}\right) e^{-\frac{\beta I}{\mu_{\max}}} \tag{11}$$

$$\mu(N) = \frac{N - N_{\min}}{K_s + N - N_{\min}} \tag{12}$$

where $\mu(T)$ is the growth limitation due to the water temperature, T_{opt} is the optimal water temperature at which the maximum growth rate is measured, and α_T is the exponential decay rate of $\mu(T)$ relative to the water temperature difference. $\mu(I)$ is the light limitation function, I is the light intensity, α_I is a light parameter related to the slope of the light function, $\mu_{\max}$ is the maximum growth rate, and β is the parameter determining the photo inhibition. $\mu(N)$ is the nutrient limitation function, N is the nutrient concentration, $N_{\min}$ is the nutrient threshold, and K_s is the half-saturation constant.

[25] The effects of light intensity and temperature on the growth rate during March to May are shown in Figure 12. $\mu(T)$ is low in March and April compared to the rest of the year. The shortwave radiation, which reflects the effect of light intensity on the phytoplankton, is lower in March than the annual mean value and increases in April and May. Since there is only one nutrient in the model, the nutrient limitation depends on the phosphorus concentration. In our model,

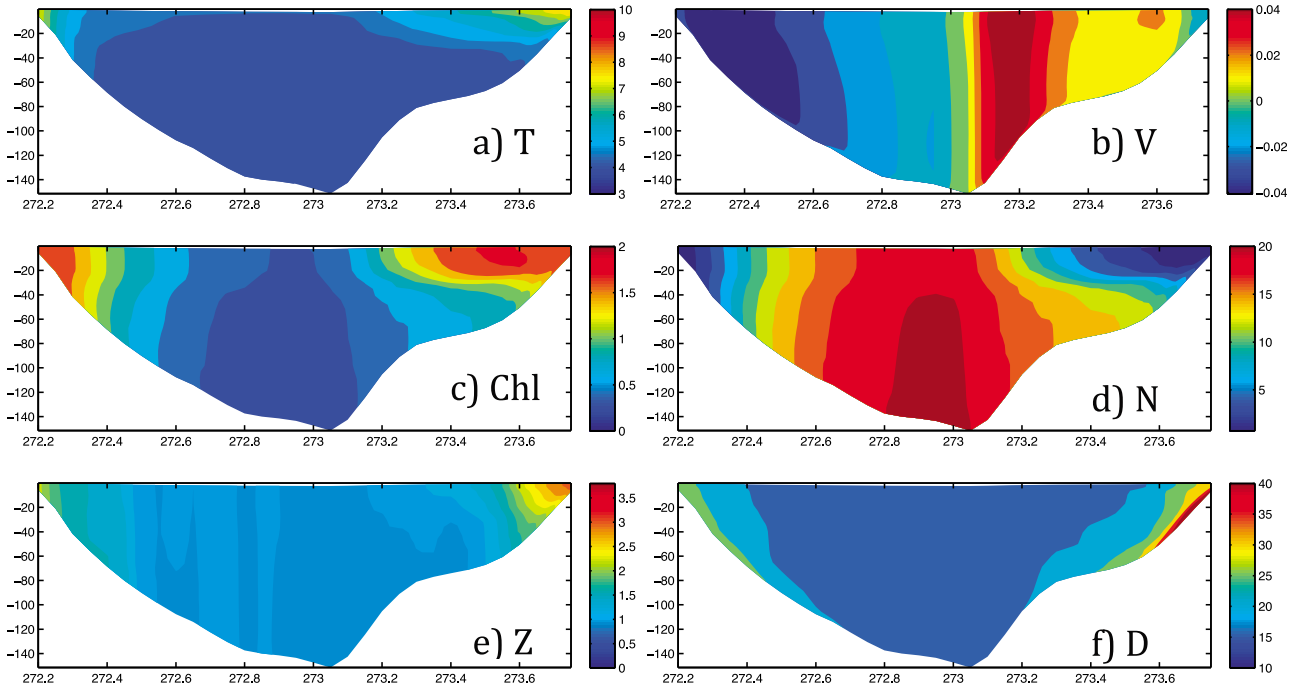

Figure 9. Simulated spatial distributions of physical and biological variables in the west-east transect in April. (a) Temperature (°C), (b) Northward velocity (m/s), (c) Chla (mg/m^3), (d) Phosphorus (mg P/m^3), (e) Zooplankton (mg C/m^3), and (f) Detritus (mg C/m^3).

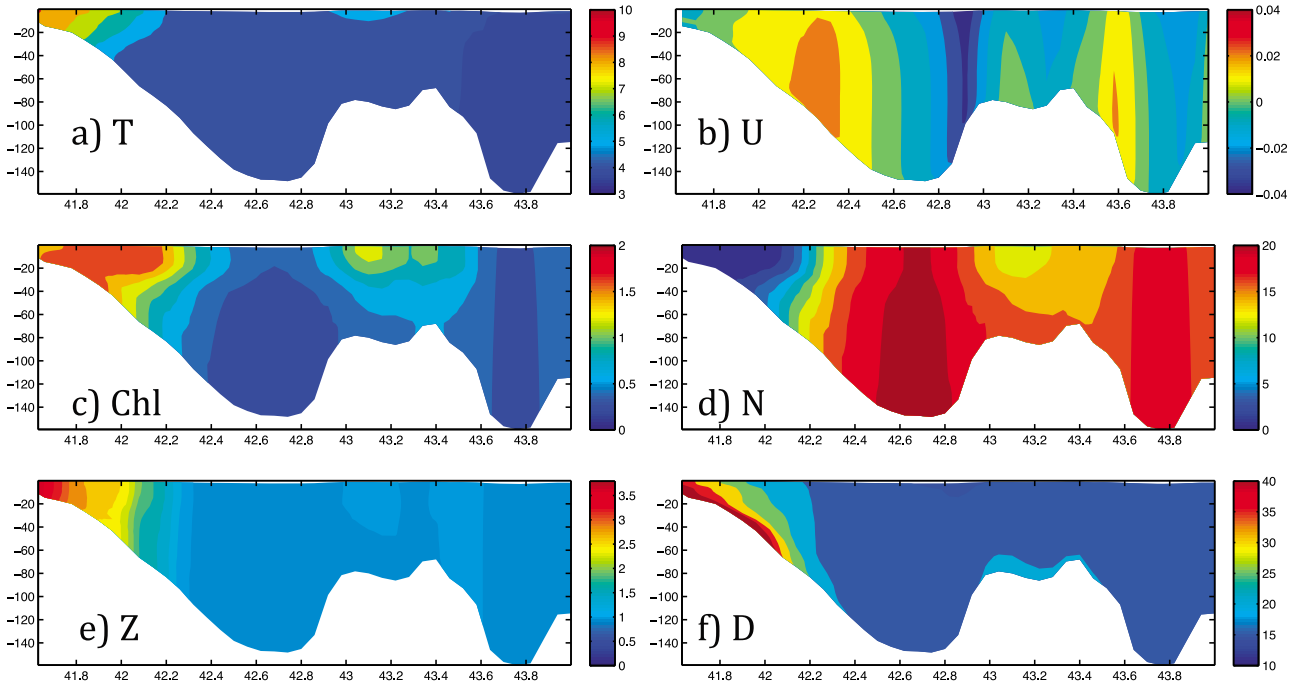

Figure 10. Simulated spatial distributions of physical biological variables in the north-south transect. (a) Temperature (°C), (b) Eastward velocity (m/s), (c) chlorophyll (mg/m^3), (d) Phosphorus (mg P/m^3), (e) Zooplankton (mg C/m^3) and (f) Detritus (mg C/m^3).

there is no external loading of nutrients from rivers and suspended sediments. Low temperature and low light intensity contribute to the low phytoplankton concentration in March. That is why no phytoplankton bloom appears in this month. In April, the light intensity increases and is higher than the annual mean value. The shallow waters warm faster than in the central basin. Like most estuaries and coastal seas around the world, the vertical mixing offers nutrients and contributes to the rapid growth of phytoplankton in shallow waters, while in deep basin, nutrients in the upper layers are not replenished to support phytoplankton growth. Even without the riverine input and suspended sediment plume, the spring bloom will appear in the coastal waters in April. Therefore the formation of the unique 'donut' phenomena is most likely due to physical mechanisms.

[26] The fronts in the Great Lakes are relatively narrow zones of enhanced horizontal gradients of physical, chemical, and biological properties [*Ullman et al.*, 1998]. The thermal fronts may last for a period of from 1 to 3 months [*Beletsky and Schwab*, 2001]. They are delimiters of water mass and play

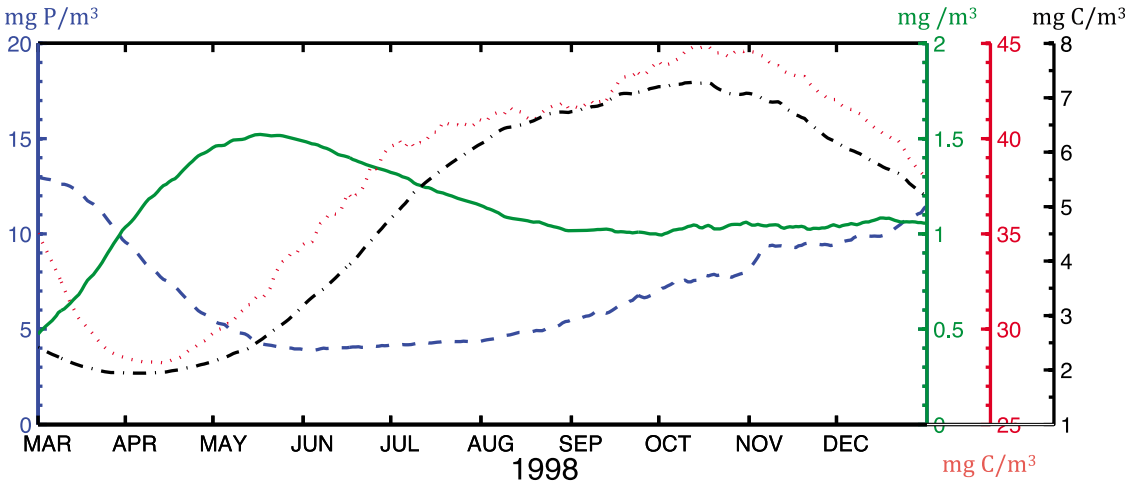

Figure 11. Time series of volume-averaged Nutrient (dashed line, mg P/m^3), Chlorophyll (solid line, mg/ m^3), Zooplankton (dash-dot line, mg C/m^3) and Detritus (dotted line, mg C/m^3) in Lake Michigan.

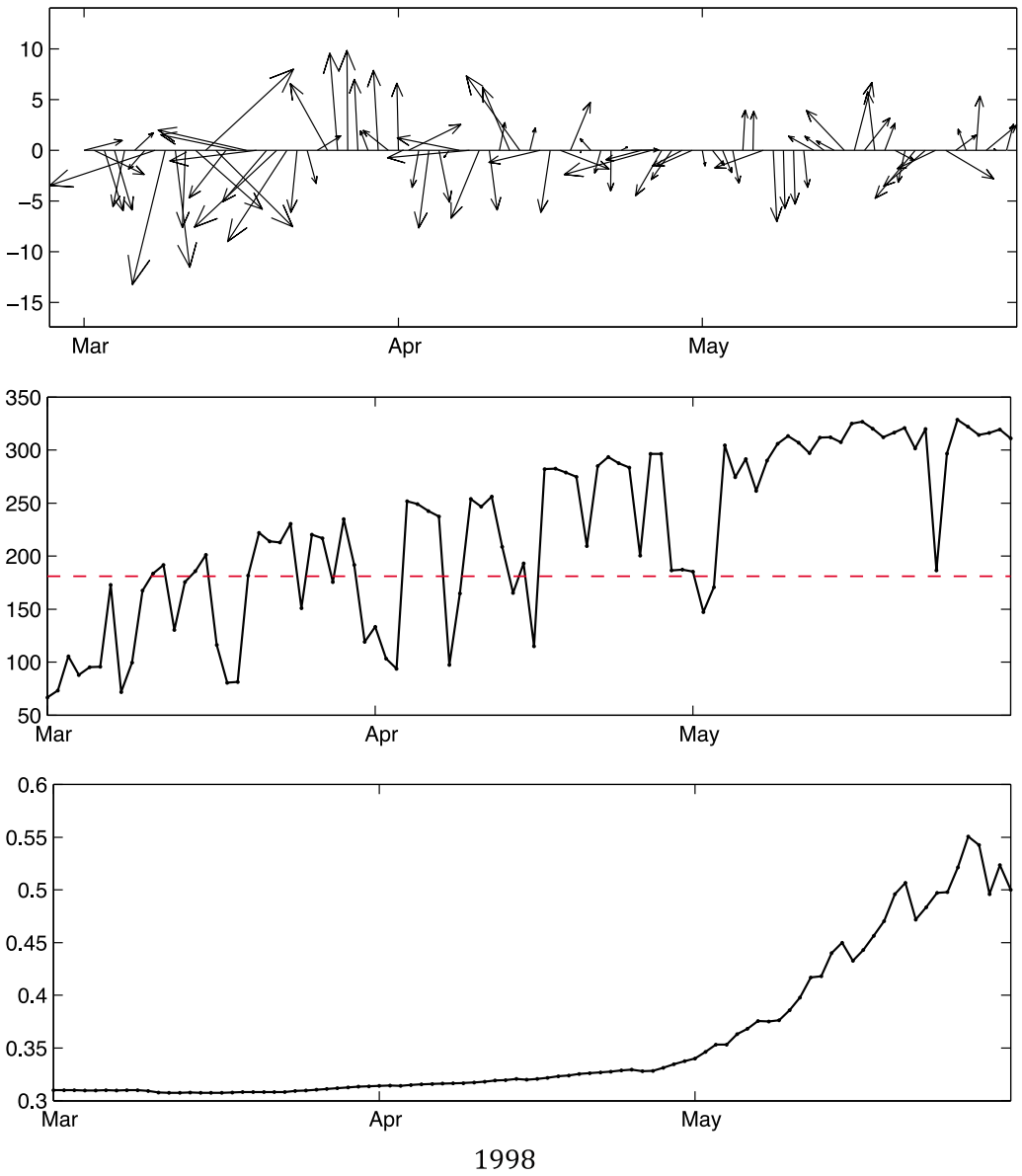

Figure 12. (top) Time series of wind vectors (m/s), (middle) shortwave radiation (W/m^2) and (bottom) effect of temperature on the phytoplankton growth μ(T) from March to May 1998.

an important role in circulation dynamics. We locate the position and intensity of the surface thermal front by calculating the gradient of simulated surface temperature (Figure 13). The intensity of thermal fronts increases from March to May. There is almost no front in SLM in March. In April, temperature gradients are about 0.15–0.2°C/km in SLM. The sharp thermal fronts inhibit the transport of phytoplankton and nutrients from inshore to offshore areas. Inshore of the thermal front, the homogeneous waters provide optimum conditions for phytoplankton growth. This agrees with the hypothesis that the timing and strength of the spring bloom is related to the timing of the thermal front [*Ullman et al.*, 1998].

[27] The cross-shore transport is important for the formation and maintenance of the structure of the 'donut' ring. A northerly wind is dominant from March to May (Figure 12, top), which drives the cyclonic current in SLM. The number of days during which the daily mean wind direction is southward in March, April, and May is 18, 19, and 15 days, respectively. The monthly mean wind speeds in the north-south direction are −1.5, −0.8 and −0.02 m/s, respectively. The cyclonic-gyre favorable wind is dominant in March and April of 1998 (Figures 9b and 10b). The gyre is stronger in March because of the stronger southward wind. The westward current appears at about 42.8°N, exactly at the position of the north edge of the phytoplankton 'donut'. Figure 14 shows the time series of westward current, temperature and Chl a concentration at a select point in this area. It is noted that even though 40% of the wind directions in March and April are northward, the westward current persists until May. The chlorophyll concentration deceases as the westward

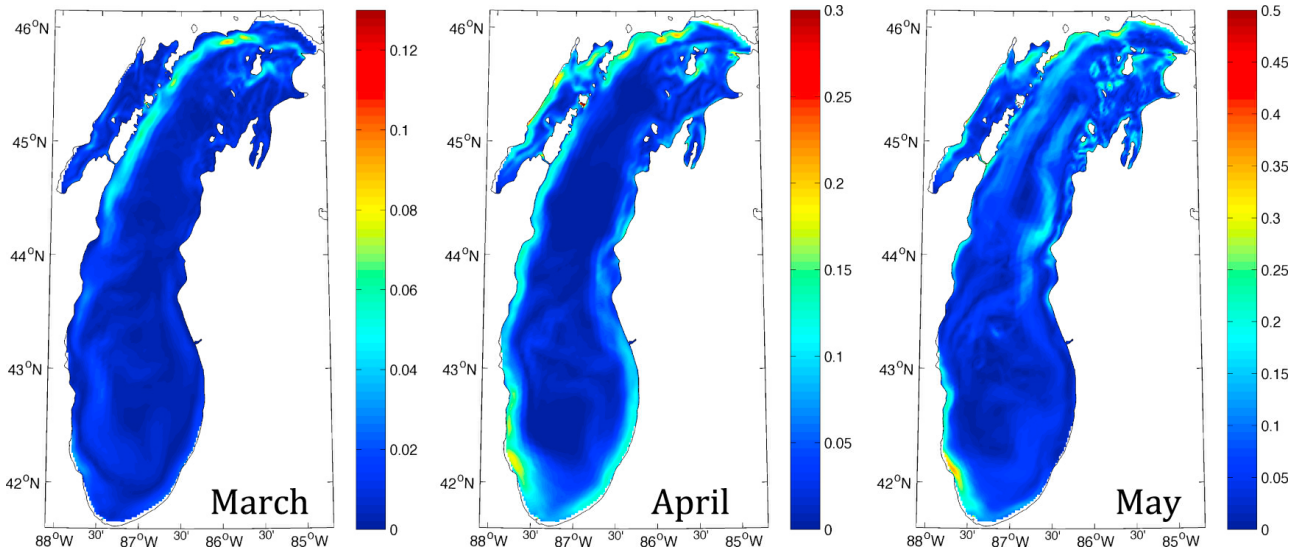

Figure 13. The intensity of thermal front calculated from the monthly averaged surface temperature (°C/km) in March, April and May 1998.

current weakens and disappears. This indicates that the high concentration of phytoplankton in the north part of the circle comes from the offshore transport of east shore areas.

5. Conclusions and Discussion

[28] A 3-D unstructured grid coupled physical-biological model is implemented to simulate the spring bloom in Lake Michigan in 1998. The model results were calibrated using in situ measurements and satellite remote sensing data. Based on the above investigations, the following conclusions can be drawn.

[29] 1. Even without nutrient input from river loading and suspended sediments, the spring bloom occurs and lasts for a time scale of 1–3 months. Therefore, the external inputs are not the only sources to provide nutrients to the spring phytoplankton bloom.

[30] 2. The coupled physical and biological processes contribute to the formation of the 'donut' structure. In spring, the increasing light intensity and water temperature favor the growth of phytoplankton. The phytoplankton in coastal shallow water rapidly grows up earlier than that in central deep basin for about 1 month, since the water in coast area warms up earlier and the light can penetrate into the lower layer.

[31] 3. The thermal front developed in coastal waters restrains the transport of the bloom and nutrients from the nearshore to deeper waters, while the wind-driven gyre circulation in southern Lake Michigan induces the significant offshore transport from the east side of SLM, both of which contribute to the establishment of a circular bloom. However, if the spring bloom depends only on the internal source of nutrients as discussed in our study, it would occur in April, but not in March. This indicates that the resuspended sediments are an important external source of nutrients for the prolonged spring bloom, but not the only source.

[32] Suspended sediments may provide nutrients for the bloom on the episodic time scales (several days) due to storm stirring. River loading may also prolong the phytoplankton bloom, which should be studied in the future.

Appendix A

[33] The mathematical expressions for each term of equations (3)–(6) are given as

$$P(uptake) = \mu^{P}_{\max} \bullet \ \mu(T) \bullet \mu(I) \bullet \mu(N)P \tag{A1}$$

$$P(respiration) = \gamma_P \bullet P \exp\left(\gamma^T \bullet T\right) \tag{A2}$$

$$Z(respiration) = \gamma_Z \bullet Z \exp\left(\gamma^T \bullet T\right) \tag{A3}$$

$$D(remineralization) = d^R \bullet D \exp\left(\gamma^T \bullet T\right) \tag{A4}$$

$$ZP(grazing) = G_{\max} \frac{\sigma_P P}{1 + \sigma_P P + \sigma_D D} Z \tag{A5}$$

$$ZD(grazing) = G_{\max} \frac{\sigma_D D}{1 + \sigma_P P + \sigma_D D} Z \tag{A6}$$

$$P(mortality) = \varepsilon_P P \tag{A7}$$

$$Z(mortality) = \varepsilon_Z Z \tag{A8}$$

$$P(sinking) = -w_P \frac{\partial P}{\partial z} \tag{A9}$$

$$D(sinking) = -w_D \frac{\partial D}{\partial z} \tag{A10}$$

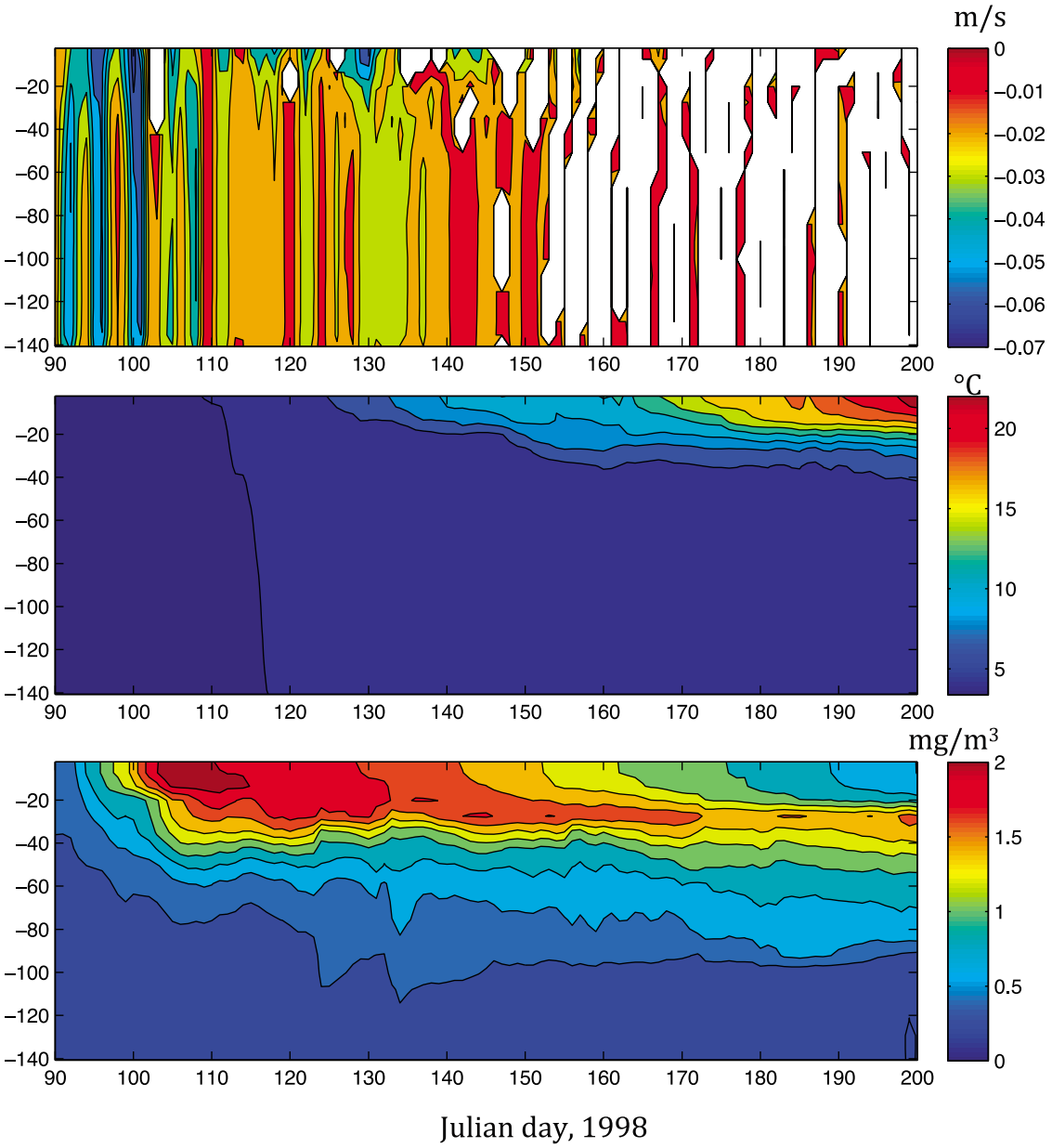

Figure 14. (top) Time series of westward velocity (m/s), (middle) temperature (°C) and (bottom) chlorophyll concentration (mg/m^3).

where the definition of each parameter in the equations (A1)–(A10) is given in Table 1.

[34] **Acknowledgments.** We appreciate support from EPA Great Lakes Restoration Initiative to the climate change project awarded to B. Lofgren and J. Wang. Thanks also goes to Cathy Darnell for editing a draft. This is GLERL Contribution 1639.

References

Beletsky, D., and D. J. Schwab (2001), Modeling circulation and thermal structure in Lake Michigan: Annual cycle and interannual variability, *J. Geophys. Res.*, *106*(C9), 19,745–19,771, doi:10.1029/2000JC000691.

Beletsky, D., J. H. Saylor, and D. J. Schwab (1999), Mean circulation in the Great Lakes, *J. Great Lakes Res.*, *25*(1), 78–93, doi:10.1016/S0380-1330(99)70718-5.

Beletsky, D., D. J. Schwab, P. J. Roebber, M. J. McCormick, G. S. Miller, and J. H. Saylor (2003), Modeling wind-driven circulation during the March 1998 sediments resuspension event in Lake Michigan, *J. Geophys. Res.*, *108*(C2), 3038, doi:10.1029/2001JC001159.

Bolgrien, D. W., and A. S. Brooks (1992), Analysis of thermal features of Lake Michigan from AVHRR satellite images, *J. Great Lakes Res.*, *18*(2), 259–266, doi:10.1016/S0380-1330(92)71293-3.

Budd, J. W., W. C. Kerfoot, S. Green, and M. Julius (2002), Donuts in the Desert? Winter production in Lake Michigan shows unexpected vertical structure, *Ocean Color Spectrum*, *Spring-Summer*, 33–34.

Chen, C., et al. (2002), A model study of the coupled biological and physical dynamics in Lake Michigan, *Ecol. Modell.*, *152*, 145–168, doi:10.1016/S0304-3800(02)00026-1.

Chen, C., L. Wang, R. Ji, J. W. Budd, and D. J. Schwab (2004), Impacts of suspended sediment on the ecosystem in Lake Michigan: A comparison between the 1998 and 1999 plume events, *J. Geophys. Res.*, *109*, C10S05, doi:10.1029/2002JC001687.

Chen, C., R. C. Beardsley, and G. Cowles (2006), An Unstructured-Grid, Finite-Volume Coastal Ocean Model (FVCOM) System, *Oceanography*, *19*(1), 78–89, doi:10.5670/oceanog.2006.92.

Hu, H., and J. Wang (2010), Modeling effects of tidal and wave mixing on circulation and thermohaline structures in the Bering Sea: Process studies, *J. Geophys. Res.*, *115*, C01006, doi:10.1029/2008JC005175.

Ji, R., et al. (2002), Influences of suspended sediments on the ecosystem in Lake Michigan: A 3-D coupled bio-physical modeling experiment, *Ecol. Modell.*, *152*, 169–190, doi:10.1016/S0304-3800(02)00027-3.

Ji, R., C. Davis, C. Chen, and R. Beardsley (2008), Influence of local and external processes on the annual nitrogen cycle and primary productivity on Georges Bank: A 3-D biological-physical modeling study, *J. Mar. Syst.*, *73*, 31–47, doi:10.1016/j.jmarsys.2007.08.002.

Kerfoot, W. C., J. W. Budd, S. A. Green, J. B. Cotner, B. A. Biddanda, D. J. Schwab, and H. A. Vanderploeg (2008), Doughnut in the desert: Late-winter production pulse in southern Lake Michigan, *Limnol. Oceanogr.*, *53*(2), 589–604, doi:10.4319/lo.2008.53.2.0589.

Mellor, G. L., and T. Yamada (1982), Development of a turbulence closure model for geophysical fluid problem, *Rev. Geophys.*, *20*, 851–875, doi:10.1029/RG020i004p00851.

Tarapchak, S. J., and C. Rubitschun (1981), Comparisons of soluble reactive phosphorus and orthophosphorus concentrations at an offshore station in southern Lake Michigan, *J. Great Lakes Res.*, *7*(3), 290–298, doi:10.1016/S0380-1330(81)72057-4.

Ullman, D., J. Brown, P. Comillon, and T. Mavor (1998), Surface temperature front in the Great Lakes, *J. Great Lakes Res.*, *24*(4), 753–775, doi:10.1016/S0380-1330(98)70860-3.

Vanderploeg, H. A., et al. (2007), Anatomy of the recurrent coastal sediment plume in Lake Michigan and its impacts on light climate, nutrients, and plankton, *J. Geophys. Res.*, *112*, C03S90, doi:10.1029/2004JC002379.

Vanderploeg, H. A., S. A. Pothoven, G. L. Fahnenstiel, J. F. Cavaletto, J. R. Liebig, C. A. Stow, T. F. Nalepa, C. P. Madenjian, and D. B. Bunnell (2012), Seasonal zooplankton dynamics in Lake Michigan, 1994–2008: Disentangling the impacts of top-down and bottom-up mechanisms during a critical ecosystem transision, *J. Great Lakes Res.*, *38*, 336–352, doi:10.1016/j.jglr.2012.02.005.

Wang, J. (1996), Global linear stability of the two-dimensional shallow-water equations: Application of the distributive theorem of roots for polynomials on the unit circle, *Mon. Weather Rev.*, *124*(6), 1301–1310, doi:10.1175/1520-0493(1996)124<1301:GLSOTT>2.0.CO;2.

Wang, J., H. Hu, D. Schwab, G. Leshkevich, and D. Beletsky (2010), Development of the Great Lakes Ice-circulation Model (GLIM): Application to Lake Erie in 2003–2004, *J. Great Lakes Res.*, *36*, 425–436, doi:10.1016/j.jglr.2010.04.002.

Weisberg, R. H., and L. Y. Zheng (2006), Circulation of Tampa Bay driven by buoyancy, tides, and winds, as simulated using a finite volume coastal ocean model, *J. Geophys. Res.*, *111*, C01005, doi:10.1029/2005JC003067.

Yang, Z., and T. Khangaonkar (2008), Modeling of Salt Intrusion, Intertidal Mixing, and Circulation in a Braided Estuary, *J. Coastal Res.*, *52*, 171–180, doi:10.2112/1551-5036-52.sp1.171.